Available online at www.sciencedirect.com
SCIENCE DIRECT®
Journal of Catalysis 222 (2004) 250–254
JOURNAL OF CATALYSIS
www.elsevier.com/locate/jcat

The role of iron carbide in multiwalled carbon nanotube growth

Andreas K. Schaper,[a,*] Haoqing Hou,[b,c] Andreas Greiner,[c] and Fritz Phillipp [d]

[a] *Center for Materials Sciences, Philipps University, 35032 Marburg, Germany*
[b] *Department of Polymer Science, University of Akron, OH 44325–3909, USA*
[c] *Department of Chemistry, Philipps University, 35032 Marburg, Germany*
[d] *Max Planck Institute for Metal Research, 70569 Stuttgart, Germany*

Received 29 July 2003; revised 20 October 2003; accepted 20 November 2003

Abstract

The pyrolysis of organometallic precursors followed by a catalyst-assisted transformation of carbon into graphite is one successful route toward the high-yield production of aligned carbon nanotubes (CNTs) with well-defined dimensions and structure. In this work we have studied the particular growth mechanisms of multiwalled CNTs synthesized from FePc and $FeCp_2$ as precursors in the pyrolysis process. TEM investigations including in situ heating experiments enabled us to directly observe the surface segregation of graphite at the expense of the encapsulated catalyst material. The observations suggest that the structural growth process is determined by the dissolution of carbon in the quasi-liquid catalyst particle, its diffusion through the particle, and its segregation in the form of graphene layers in the case of supersaturation. These processes were proved to occur via the formation of an intermediate iron carbide phase. The results also demonstrated how the increasing expulsory forces may cause the gradual displacement of the fluid catalyst during nanotube growth.

Keywords: Multiwalled carbon nanotubes; Growth mechanisms; Iron carbide intermediate; Transmission electron microscopy; In situ heating observations

1. Introduction

The catalytic approach (see review by de Jong and Geus [1]) has been recognized as a promising way toward the large-scale production of multiwalled and single-walled carbon nanotubes (MWCNTs, SWCNTs) and, even more importantly, toward a better control of the anisotropic dimensions, the helicity, and the alignment of the tubes. The main routes pursued of the catalytic CNT synthesis are: (i) decomposition and chemical vapor deposition (CVD) of lower hydrocarbons on preformed catalytically active substrates [2–4] and its plasma-enhanced variant [5], (ii) pyrolysis of an organometallic precursor on a transition metal salt along with a reactant hydrocarbon as additional or as the only carbon source [6–8], (iii) synthesis from polymer precursors in the presence of a metallic catalyst [9].

The diffusion of carbon through the catalyst particle and its segregation in the form of ordered graphene layers have been suggested as key processes in both the base growth and the tip growth mechanism of carbon filaments and nanotubes [10]. In case of iron, irrespective of the well-known iron/carbon phase diagram for the macroscopic bulk material [11], the amount of carbon that can generally be incorporated into the high-temperature quasi-liquid nanoparticle is not well known. About 50 at.% carbon were measured in melted iron particles by Krivoruchko and Zaikovskii [12], and recently Jourdain et al. [13] estimated from their computer image analysis of transmission electron microscope (TEM) images a carbon atomic ratio of even $x_C \sim 0.68$ in Ni/Fe metal particles.

There are several reports about the occurrence of iron and other carbides in the CNT products from the pyrolysis of different precursor materials as well as using the arc discharge method [14–21]. However, the role metal carbides play in the synthesis of the various forms of carbon nanotubes and nanoparticles is a matter of debate. While, e.g., the catalytic activity of pure Fe_3C in the decomposition and pyrolysis of acetylene has been proved negligible [22], its function as an intermediate in the transformation of amorphous carbon into graphite is still controversial [13,23,24]. Recently, evidence of the iron carbide phase (cementite) participating in the graphitization of amorphous carbon has been presented

* Corresponding author.
E-mail address: schaper@staff.uni-marburg.de (A.K. Schaper).

0021-9517/$ – see front matter
doi:10.1016/j.jcat.2003.11.011

by Pérez-Cabero et al. [25] using X-ray diffraction investigations, and by Sinclair et al. [26] in an electron microscopy and diffraction analysis.

In the present study we have performed in situ TEM observations of MWCNTs prepared from iron(II)–phthalocyanine, and from ferrocene/anthracene mixtures as catalyst precursors. Even if the true mechanisms of the nanotube growth regime cannot actually be simulated in the microscope, heating experiments have provided us with valuable information about the initiation and growth of carbon nanotubes. The new experiments convincingly evidence the role of an iron carbide intermediate phase in the formation of graphite layers constituting MWCNTs.

2. Experimental

A dual high-temperature furnace, equipped with a two-stage tubular quartz reactor and independent temperature controllers, was used for the experiments. Multiwalled carbon nanotubes were synthesized using (i) the iron-containing precursor iron (II) phthalocyanine (FePc) ($C_{32}H_{16}FeN_8$, ca. 90% dye content; Aldrich) which served as the carbon and catalyst source in one, and (ii) ferrocene ($FeCp_2$) ($C_{10}H_{10}Fe$; 98%; Acros Organics) as catalyst precursor along with anthracene ($C_{14}H_{10}$; 98%; Aldrich) as an additional carbon source [27]. The FePc, 0.3 g in a quartz boat at the lower temperature part in the tubular quartz reactor, was vaporized at 550 °C, the vapor was then carried by an Ar/H_2 (volume ratio 1/1) nominal flow of 430 ml/min into the higher temperature region of the reactor, where the pyrolytic decomposition of the vapor occurred at about 900 °C. (Because of the temperature gradients present in the reactor tube, the given temperatures are average values.) The pyrolysis products were deposited on a silicon substrate, located at the higher temperature part of the reactor. For comparison, lower vaporization and pyrolysis temperatures of ca. 160 and 700 °C, respectively, were suitable in case of nanotube growth from a $FeCp_2$/anthracene mixture. The gas flow was similar in both cases.

For TEM, about 2–3 mg of the mat-like nanotube material, collected from the silicon substrate, was dispersed in 10 ml ethanol (99%, Aldrich) by sonication. The CNTs were picked up from the suspension using copper grids covered with holey carbon film. The microscopic investigations were performed in a Jeol JEM 3010 high-resolution transmission electron microscope (HRTEM) operated at 300 kV and equipped with a 2k × 2k slow scan CCD camera (Gatan). In situ structural studies at elevated temperatures were carried out using the Jeol high-voltage transmission electron microscope (HVTEM) ARM 1250 at the Max Planck Institute of Metal Research in Stuttgart, Germany, which is equipped with a side-entry heating stage and a drift-compensated video-recording system [28].

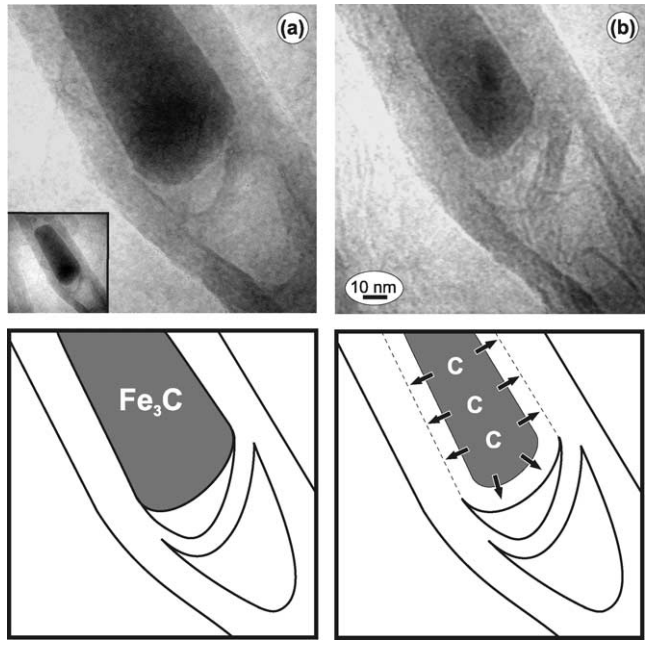

Fig. 1. In situ HVTEM of the structural changes of an encapsulated catalyst particle at the tip of a CNT, and of the surrounding CNT walls at a temperature of ca. 875 °C. (a) and (b) Micrographs of the rear part of the particle shown in the inset at a time interval of 3.5 min, along with the corresponding schematic drawings of the changes observed.

3. Results

3.1. In situ observations

Applying FePc as the precursor, we typically obtained rather straight nanotubes with a high degree of graphitic ordering in the tube walls [29]. Usually, at the top end of each CNT the metal particle is found that has initiated the tube formation. Depending on the growth and deposition conditions, the tube tip is either open (Figs. 1 and 2), or even completely closed by curved graphene layers (Fig. 3), and there is a variation in the extent of internal transverse carbon bridging (bamboo structure). The two photographs in Figs. 1a and 1b are from an in situ heating sequence in the electron microscope showing, in greater detail, the changes of the core particle and the surrounding graphitic sheath of the tube tip displayed in the inset. The micrographs were taken at a specimen temperature of approximately 875 °C at a time interval of 3.5 min. The relevant observations depicted in the corresponding schematic drawings are the formation of a new ca. 10-nm-thick transverse carbon bridge by segregation of graphene layers at the rear surface of the filling particle, and the inward directed thickness growth of the CNT walls by graphitic segregation at the particle side surfaces. It is important to note that during these structural transformations the outer CNT diameter remained almost constant; i.e., the thickening of the graphitic tube wall occurred entirely at the expense of the encapsulated material. Hence, because there is no other carbon source due to the high vacuum, the conclusion can be drawn that the carbon segregating in the

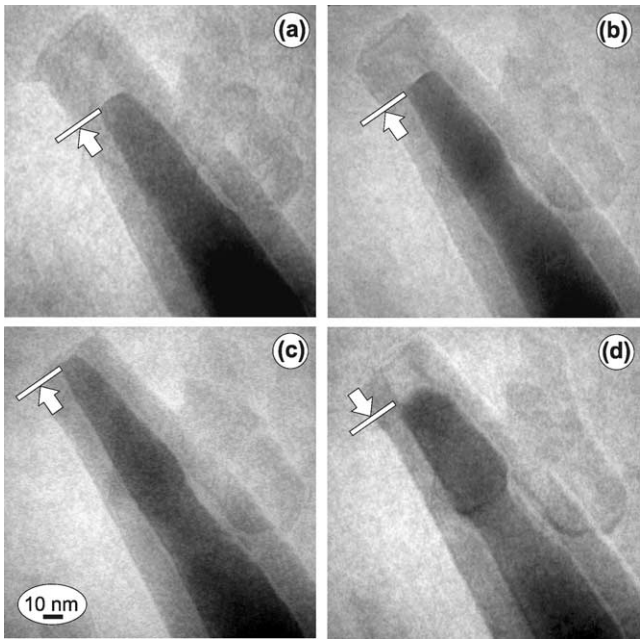

Fig. 2. (a) to (d) Displacement of the core material through the CNT capillary and neck formation as a result of the buildup of expulsory forces due to graphite segregation at the catalyst surface in an in situ HVTEM image sequence. Time interval between (a) and (d) ca. 25 s at 880 °C.

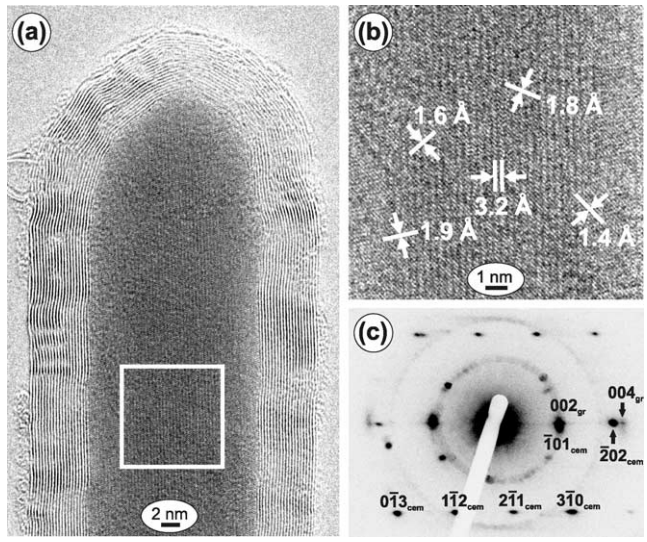

Fig. 3. (a) TEM micrograph of a tip of a FePc-synthesized MWCNT capped by graphite layers continuously enclosing the encapsulated catalyst material; (b) close-up of the area marked in (a) exhibiting different lattice fringes; (c) SAED pattern that includes the characteristic graphite scattering of the nanotube overlapped by the [131] zone axis diffraction pattern of the cementite core.

form of graphite at the outer particle surface undoubtedly stems from the bulk of the particle. Furthermore, it must be concluded that this amount of carbon must have been contained in the as-grown original particle already at room temperature before the beginning of the in situ microscopy experiments.

Beyond a temperature of about 860 °C, under the high-energy electron irradiation, a point is reached where the core material melts and rapidly moves along the tube axis as documented in the time-resolved picture series in Fig. 2. Starting at Fig. 2a, after a time interval of ca. 9 s the core has reached the capillary open end (Fig. 2c) and some material is expulsed. Fig. 2d shows the situation another 17 s later when the remaining part of the core is sucked back into the tube accompanied by a pronounced neck formation in the liquid particle. We could observe several repeats of this displacement process until the core material was completely ejected.

3.2. Structure determination of the core material

If it is true that, at least, a portion of the carbon dissolved in the metal particle is stored there even during cooling the deposited pyrolysis product to room temperature, the question arises as to the nature of the low-temperature carbon-in-metal phase. An answer will be possible on the basis of the electron microscope and diffraction investigations described in the following.

The electron micrograph in Fig. 3a shows the tip of a FePc-pyrolyzed MWCNT formed by nearly 20 graphene layers, and neatly filled over a larger distance with iron-containing foreign material. The nanotube tip is perfectly covered and closed by continuously curved graphene layers. A higher magnification view of the inner core region marked in Fig. 3a is provided in Fig. 3b. The image reveals different sets of lattice planes within the enclosed material with one prominent fringe spacing of about 3.2 Å aligned almost parallel to the graphitic layering and thus to the tube axis. Fig. 3c represents a selected area electron diffraction (SAED) pattern that covers the corresponding area of the encapsulated material shown in Fig. 3b together with parts of the graphitic tube. Therefore, with the well-defined c spacing of graphite, we have a precise standard for the Bragg reflections to be identified. The graphite scattering including the characteristic equatorial (00l) reflections as well as the streak-like (100) scattering of the graphite layers, along with the corresponding faint (hk0) ring pattern, is overlapped by quite a sharp spot pattern of a highly crystalline phase. Evaluation of this pattern shows that it closely agrees with the [131] zone axis diffraction of the iron carbide Fe_3C phase (cementite), several (h0l) and (h1l) reflections of which are indexed in Fig. 3b. However, presupposing a reasonable (002) graphitic layer spacing of 3.45 Å, a discrepancy of about 0.35 Å exists between the (101) lattice spacing of 3.383 Å obtained from the results of X-ray scattering measurements in the literature [30], and the value of 3.74 Å determined here. Increasing lattice parameters are compatible with a lattice expansion due to a carbon content exceeding that of the pure Fe_3C phase, thus indicating supersaturation.

In a previous paper, the occurrence of an iron carbide phase has been identified also in CNTs catalytically grown from iron(III)chloride at temperatures in the range 750–

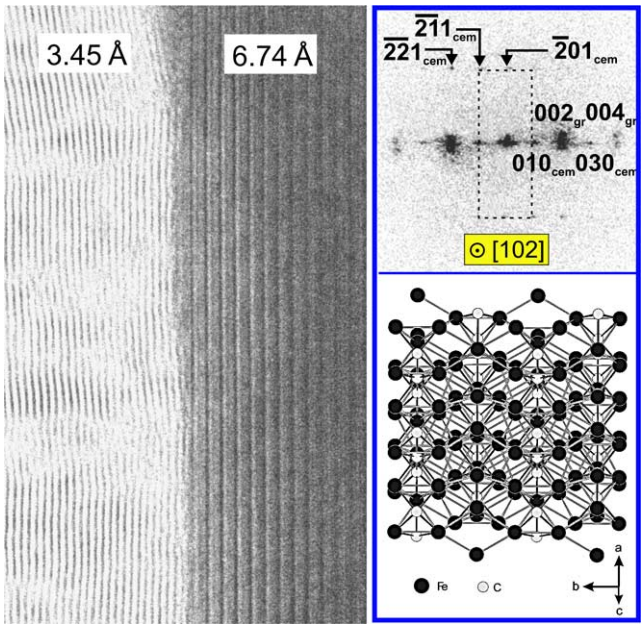

Fig. 4. Lattice fringe image of the interface region between the graphitic wall and the encapsulated material in a MWCNT prepared from ferrocene/anthracene precursor showing the (002) and (010) lattice planes of graphite and cementite, respectively. The power spectrum clearly reveals the diffraction of Fe_3C down [102] overlapped by the graphitic tube scattering; the corresponding structure model of cementite illustrates the preferred alignment of the two phases.

1100 °C [31]. Another proof comes from the pyrolysis of ferrocene/anthracene precursor material [27]. The micrograph in Fig. 4 shows a close-up lattice fringe image of the interface region between the multilayer tube wall and the enclosed filling material. While the characteristic (002) graphite *c*-layer spacing of 3.45 Å is seen on the left-hand side, on the right a fringe pattern with a spacing of about twice that value is revealed. The latter very closely corresponds to the 6.741 Å of the X-ray *b*-axis lattice parameter of cementite [30]. In the power spectrum of the image that includes both structures one can clearly distinguish between the graphite (002) and (004) reflections and the $(0l0)$ $(l = 1, 2, 3)$ reflections of the carbide phase. (The extra off-equatorial spot detected near the (004) equatorial reflection is due to the upper part of the graphitic wall deviating slightly in orientation). Besides the equatorial scattering, there are additional reflections relating to $\{2k1\}$ $(k = \pm 0, 1, 2, \ldots)$ lattice planes of the orthorhombic unit cell when locking down the [102] direction. Accordingly, in this particular case a well-defined crystal orientational relationship $[010]_{carbide} \parallel [002]_{graphite}$ exists between the two phases which appears quite favorable from the structure model of cementite in Fig. 4. There are indications that the growth of the carbon nanotube, i.e., the growth of curved graphene layers, originates from such a straight parallel alignment between both lattices along a low index plane.

4. Discussion

The electron microscope in situ heating experiments presented in this paper could not mimic, of course, the CNT growth process in its true nature because of the lack of continued carbon supply from decomposition of a precursor. Nevertheless, the observed structural phase changes under heat have revealed a number of particular aspects of the growth mechanism of carbon nanotubes.

First, the images of graphite segregation at the surface of the catalyst particle under vacuum conditions support the validity of the concept of dissolution of carbon in the metal catalyst and of the carbon-through-metal diffusion. The thickness growth of the nanotube walls during heating is clear evidence of a considerable amount of carbon contained in the metallic nanoparticle. This carbon amount serves, in the in situ experiment, as the only reservoir for the creation of new graphene layers. (The "new layers" probably represent parts of one and the same scrolled graphene layer forming the CNT [29].) With this reservoir getting used up, the graphitic segregation stops and the remaining core material gets stuck in the inner part of the tube. In the real growth process, periodic fluctuations of the carbon concentration in the catalyst are made responsible for the bamboo-like growth of MWCNTs with its characteristic axial structure periodicity [13]. Tube growth takes place when the carbon concentration in the particle exceeds supersaturation. Repeated decreases of the amount of carbon due to its consumption for the graphite segregation should be associated with increasing surface tension at the tube/catalyst interface [13,34]. These surface tensional forces as well as the compressive stress accumulated in the graphitic sheath in consequence of the growth of new graphene layers at the inside of the tube cause the observed progressive ejection as well as the neck formation of the liquid particle (compare [13,34,35]). The competition between the expulsary forces and the interfacial capillary forces has a strong influence on the growth rate in the length direction and also the bamboo shaping of the MWCNTs.

Second, the clear identification of the cementite phase suggests the participation of iron carbide intermediates in the transformation of carbon into graphite. The in situ segregation of graphitic layers from cementite can be explained by its decomposition into metal and carbon as proved possible even at temperatures around 500 °C by Podgurski et al. [33]. The high-energy irradiation has probably an accelerating effect on the decomposition. Whether only Fe_3C or even the more carbon-rich phases Fe_2C and FeC are involved in the tube growth remains open. Our observations concern the frozen-in situation of the particle, and there is no precise information about the original carbon concentration at high temperatures. A hot liquid-like metal particle possesses an enormous capacity of carbon uptake which inevitably decreases when the particle is cooled down [32]. Considering an estimated amount of 50 at.% of carbon and more [12,13], carbon-rich carbides are rather likely to exist at elevated temperatures. The carbon nanotubes reported here were ob-

viously grown via a supersaturated carbide phase mediating the carbon-through-metal transmission. The new graphene layers were preferentially segregated parallel to low-index lattice planes of the carbide which seems to be one reason for the rather frequent formation of polygonized MWCNT cross sections. On the other hand, the detection of cubic α-iron particles within CNTs after a low-temperature growth process [31] suggests that carbon does not necessarily form a carbide phase with the iron host. This issue, however, has not yet been cleared up under actual growth conditions. Hence, even in the context of the present results, the occurrence of a disordered solid solution of carbon in iron must be taken into consideration, besides the existence of a metallic carbide phase.

Third, the carbon-saturated metallic nanoparticle melts at temperatures far below the bulk melting point of the metal or carbide. One reason for this melting point reduction is the well-documented size effect [36], other reasons are the weakening and even rupture of bonds between the metal atoms because of the interaction with the dissolved carbon [9,12], and the enhancement of those reactions by the effect of electron irradiation [37].

5. Conclusions

In this paper we have shown that iron carbide instead of metallic iron is, at least partially, involved in the CNT growth from different iron precursors; i.e., carbon is chemically bound within the catalyst in a rather stabilized form, namely Fe_3C. The in situ electron microscopy studies revealed the role of the carbide phase as an intermediate in the catalyst-mediated graphite formation by promoting the successive segregation of well-ordered new graphene layers on its surface. Thereby, axial movement of the quasi-liquid material inside the tube due to the buildup of compressive stress during thickness growth of the graphitic tube wall, and due to increasing surface tensional forces between the core material and the tube, illustrates how progress in nanotube growth is provided.

Acknowledgment

We thank R. Hoeschen, Max Planck Institute for Metal Research, Stuttgart, for his expert technical assistance.

References

[1] K.P. de Jong, J.W. Geus, Catal. Rev. Sci. Eng. 42 (2000) 481.
[2] M. Terrones, W.K. Hsu, A. Schilder, H. Terrones, N. Grobert, J.P. Hare, Y.Q. Zhu, M. Schwoerer, K. Prassides, H.W. Kroto, D.R.M. Walton, Appl. Phys. A 66 (1998) 307.
[3] S. Fan, M.G. Chapline, N.M. Franklin, T.W. Tombler, A.M. Cassell, H. Dai, Science 283 (1999) 512.
[4] N. Grobert, M. Terrones, S. Trasobares, K. Kordatos, H. Terrones, J. Olivares, J.P. Zhang, Ph. Redlich, W.K. Hsu, C.L. Reeves, D.J. Wallis, Y.Q. Zhu, J.P. Hare, A.J. Pidduck, H.W. Kroto, D.R.M. Walton, Appl. Phys. A 70 (2000) 175.
[5] Z.F. Ren, Z.P. Huang, J.W. Xu, J.H. Wang, P. Bush, M.P. Siegal, P.N. Provencio, Science 282 (1998) 1105.
[6] S. Huang, L. Dai, A.W.H. Mau, J. Phys. Chem. B 103 (1999) 4223.
[7] M. Terrones, P.M. Ajayan, F. Banhart, X. Blase, D.L. Carroll, J.C. Charlier, R. Czerw, B. Foley, N. Grobert, R. Kamalakaran, P. Kohler-Redlich, M. Rühle, T. Seeger, H. Terrones, Appl. Phys. A 74 (2002) 355.
[8] Ph. Mauron, Ch. Emmenegger, A. Züttel, Ch. Nützenadel, P. Sudan, L. Schlapbach, Carbon 40 (2002) 1339.
[9] N.I. Maksimova, O.P. Krivoruchko, G. Mestl, V.I. Zaikovskii, A.L. Chuvilin, A.N. Salanov, E.B. Burgina, J. Mol. Catal. A: Chem. 158 (2000) 301.
[10] R.T.K. Baker, Carbon 27 (1989) 315.
[11] T.B. Massalski, J.L. Murray, L.H. Bennett, H. Baker (Eds.), Binary Alloy Phase Diagrams, American Society for Metals, Metal Park, OH, 1986.
[12] O.P. Krivoruchko, V.I. Zaikovskii, Kinet. Catal. 39 (1998) 607.
[13] V. Jourdain, H. Kanzow, M. Castignolles, A. Loiseau, P. Bernier, Chem. Phys. Lett. 364 (2002) 27.
[14] A. Oberlin, M. Endo, T. Koyama, J. Cryst. Growth 32 (1976) 335.
[15] A. Sacco, P. Thacker, T.N. Chang, A.T.S. Chiang, J. Catal. 85 (1984) 224.
[16] A.J.H.M. Kock, P.K. de Bokx, E. Boellaard, W. Klop, J.W. Geus, J. Catal. 96 (1985) 468.
[17] I. Stewart, M.J. Tricker, J.A. Cairns, J. Catal. 94 (1985) 360.
[18] C. Guerret-Plécourt, Y. Le Bouar, A. Loiseau, H. Pascard, Nature 372 (1994) 761.
[19] Y. Saito, Carbon 33 (1995) 979.
[20] J. Gavillet, A. Loiseau, J. Thibault, A. Maigné, O. Stephan, 1. Physics and Materials, in: Proc. 15th Int. Congr. Electron Microscopy, Durban, SA (1–6 Sept. 2002), Microscopy Society of Southern Africa, 2002, p. 201.
[21] N. Grobert, M. Terrones, A.J. Osborne, H. Terrones, W.K. Hsu, S. Trasobares, Y.Q. Zhu, J.P. Hare, H.W. Kroto, D.R.M. Walton, Appl. Phys. A 67 (1998) 595.
[22] K. Hernadi, A. Fonseca, J.B. Nagy, Á. Fudala, D. Bernaerts, I. Kiricsi, Appl. Catal. A: G 228 (2002) 103.
[23] W.L. Holstein, J. Catal. 152 (1995) 42.
[24] H. Kanzow, A. Ding, Phys. Rev. B 60 (1999) 11180.
[25] M. Pérez-Cabero, I. Rodríguez-Ramos, A. Guerrero-Ruíz, J. Catal. 215 (2003) 305.
[26] R. Sinclair, T. Itoh, R. Chin, Microsc. Microanal. 8 (2002) 288.
[27] H. Hou, A.K. Schaper, F. Weller, A. Greiner, Chem. Mater. 14 (2002) 3990.
[28] R. Höschen, W. Sigle, F. Phillipp, in: Proc. EUREM-11, Dublin, Ireland (26–30 August 1996), Committee Europ. Soc. Microscopy, Brussels (Belgium), 1998, I 373/374.
[29] W. Ruland, A.K. Schaper, H. Hou, A. Greiner, Carbon 41 (2003) 423.
[30] D. Fruchart, P. Chaudouet, R. Fruchart, A. Rouault, J.P. Senateur, J. Solid State Chem. 51 (1984) 246.
[31] H. Hou, A.K. Schaper, Z. Jun, F. Weller, A. Greiner, Chem. Mater. 15 (2003) 580.
[32] V.V. Kovalevski, A.N. Safronov, Carbon 36 (1998) 963.
[33] H.H. Podgurski, J.T. Kummer, T.W. DeWitt, P.H. Emmett, J. Amer. Chem. Soc. 72 (1950) 5382.
[34] X.X. Zhang, Z.Q. Li, G.H. Wen, K.K. Fung, J. Chen, Y. Li, Chem. Phys. Lett. 333 (2001) 509.
[35] L.T. Chadderton, Y. Chen, J. Cryst. Growth 240 (2002) 164.
[36] F. Benissad, P. Gadelle, M. Coulon, L. Bonnetain, Carbon 26 (1988) 425.
[37] F. Banhart, Ph. Redlich, P.M. Ajayan, Chem. Phys. Lett. 292 (1998) 554.